First clinico-pathological evidence of a non PSMA-related uptake mechanism for 68Ga-PSMA-11 in salivary glands

Rupp, Niels J ; Umbricht, Christoph A ; Pizzuto, Daniele A ; Lenggenhager, Daniela ; Töpfer, Antonia ; Müller, Julian ; Mühlematter, Urs Jacob ; Ferraro, Daniela A ; Messerli, Michael ; Morand, Grégoire B ; Huber, Gerhard F ; Eberli, Daniel ; Schibli, Roger ; Müller, Cristina ; Burger, Irene A

Abstract: The intense accumulation of PSMA radioligands in salivary glands is still not well understood. It is of concern for therapeutic applications of PSMA radioligands, as therapeutic radiation will damage these glands. A better understanding of the uptake mechanism is, therefore, crucial to allow the finding of solutions to reduce toxicity. The aim of this study was to investigate on whether or not the accumulation of PSMA-targeting radioligands in submandibular glands (SMG) can be explained with PSMA expression levels using the methods of autoradiography (ARG) and immunohistochemistry (IHC). Methods: All patients gave written informed consent for further utility of the biological material. SMG of 9 patients, pancreatic tissue of 4 patients and prostate cancer (PCA) lesions of 9 patients were analyzed. Fresh tissue specimen were analyzed by means of PSMA-IHC (using an anti-PSMA-antibody and an immunoreactivity score system - IRS) and ARG using 177Lu-PSMA-617 (with quantification of the relative signal intensity compared to a PSMA-positive standard). The SUVmax in salivary glands, pancreas and PCA tissues were quantified in 60 clinical 68Ga-PSMA-11 PET scans for recurrent disease, as well as the 9 primary tumors selected for ARG and IHC. Results: PCA tissue samples revealed a wide range of PSMA staining intensity on IHC (IRS 70–300) as well as in ARG (1.33 – 21.98%). This variability on PCA tissue could also be observed in 68Ga-PSMA-11 PET (SUVmax 4.4-16) with a significant correlation between ARG and SUVmax ($P < 0.001$, $R2 = 0.897$). On IHC, ARG and 68Ga-PSMA-11 PET, the pancreatic tissue was negative (IRS = 0, ARG = 0.1±0.05%, SUVmax of 3.1±1.1). The SMG tissue displayed only focal expression of PSMA limited to the intercalated ducts on IHC (IRS 10-15) and a minimal signal on ARG (1.3±0.9%). In contrast, all SMG showed a high 68Ga-PSMA-11 accumulation on PET scans (SUVmax 23.5±5.2). Conclusion: Our results indicate that the high accumulation of PSMA radioligands in salivary glands does not correspond to a high PSMA expression levels determined using ARG and IHC. These findings provide evidence, that the significant accumulation of PSMA radioligands in SMG is not primarily a result of PSMA-mediated uptake.

DOI: https://doi.org/10.2967/jnumed.118.222307

Huber, Gerhard F; Eberli, Daniel; Schibli, Roger; Müller, Cristina; Burger, Irene A (2019). First clinico-pathological evidence of a non PSMA-related uptake mechanism for 68Ga-PSMA-11 in salivary glands. Journal of Nuclear Medicine, 60(9):1270-1276.
DOI: https://doi.org/10.2967/jnumed.118.222307

Journal of Nuclear Medicine, published on February 8, 2019 as doi:10.2967/jnumed.118.222307

First clinico-pathological evidence of a non PSMA-related uptake mechanism for ^{68}Ga-PSMA-11 in salivary glands.

[a†]Niels J. Rupp,[b†]Christoph A. Umbricht, [c]Daniele A. Pizzuto, [a]Daniela Lenggenhager, [a]Antonia Töpfer, [c]Julian Müller, [c]Urs J. Muehlematter, [c]Daniela A. Ferraro, [c]Michael Messerli, [d]Grégoire B. Morand, [e]Gerhard F. Huber, [f]Daniel Eberli, [b]Roger Schibli, [b‡]Cristina Müller, [c‡]Irene A. Burger[*]

[a]Department of Pathology and Molecular Pathology, University Hospital Zürich, University of Zürich, Switzerland

[b]Center for Radiopharmaceutical Sciences ETH-PSI-USZ, Paul Scherrer Institute, Villigen-PSI, Switzerland

[c]Department of Nuclear Medicine, University Hospital Zürich, University of Zürich, Switzerland

[d]Department of Otorhinolaryngology - Head and Neck Surgery, University Hospital Zürich, University of Zürich, Switzerland

[e]Department of Otorhinolaryngology - Head and Neck Surgery, Kantonsspital St. Gallen, Switzerland

[f]Department of Urology, University Hospital Zürich, University of Zürich, Switzerland

[†] These authors contributed equally to the manuscript

[‡]These authors contributed equally to the manuscript

***Corresponding author:**
PD Dr. med. Irene A. Burger
Department of Nuclear Medicine, University Hospital Zürich
Rämistrasse 100
8091 Zürich
Switzerland
Phone: +41-44-2551111
Mail: Irene.burger@usz.ch

Word count: 4956

Short running title: PSMA uptake in salivary glands.

Abstract:

The intense accumulation of PSMA radioligands in salivary glands is still not well understood. It is of concern for therapeutic applications of PSMA radioligands, as therapeutic radiation will damage these glands. A better understanding of the uptake mechanism is, therefore, crucial to allow the finding of solutions to reduce toxicity. The aim of this study was to investigate on whether or not the accumulation of PSMA-targeting radioligands in submandibular glands (SMG) can be explained with PSMA expression levels using the methods of autoradiography (ARG) and immunohistochemistry (IHC).

Methods: All patients gave written informed consent for further utility of the biological material. SMG of 9 patients, pancreatic tissue of 4 patients and prostate cancer (PCA) lesions of 9 patients were analyzed. Fresh tissue specimen were analyzed by means of PSMA-IHC (using an anti-PSMA-antibody and an immunoreactivity score system - IRS) and ARG using ^{177}Lu-PSMA-617 (with quantification of the relative signal intensity compared to a PSMA-positive standard). The SUV_{max} in salivary glands, pancreas and PCA tissues were quantified in 60 clinical ^{68}Ga-PSMA-11 PET scans for recurrent disease, as well as the 9 primary tumors selected for ARG and IHC.

Results:

PCA tissue samples revealed a wide range of PSMA staining intensity on IHC (IRS 70–300) as well as in ARG (1.33 – 21.98%). This variability on PCA tissue could also be observed in ^{68}Ga-PSMA-11 PET (SUV_{max} 4.4-16) with a significant correlation between ARG and SUV_{max} ($p < 0.001$, $R^2 = 0.897$). On IHC, ARG and ^{68}Ga-PSMA-11 PET, the pancreatic tissue was negative (IRS = 0, ARG = 0.1±0.05%, SUV_{max} of 3.1±1.1). The SMG tissue displayed only focal expression of PSMA limited to the intercalated ducts on IHC (IRS 10-15) and a minimal signal on ARG (1.3±0.9%). In contrast, all SMG showed a high ^{68}Ga-PSMA-11 accumulation on PET scans (SUV_{max} 23.5±5.2).

Conclusions:

Our results indicate that the high accumulation of PSMA radioligands in salivary glands does not correspond to a high PSMA expression levels determined using ARG and IHC.

These findings provide evidence, that the significant accumulation of PSMA radioligands in SMG is not primarily a result of PSMA-mediated uptake.

Key words (MESH-keywords): Prostate cancer, Prostate-Specific Membrane Antigen, ^{177}Lu-PSMA-617, ^{68}Ga-PSMA-11, Positron Emission Tomography, immuno-histochemistry, autoradiography

INTRODUCTION:

The prostate-specific membrane antigen (PSMA) is upregulated in prostate cancer (PCA), while only a few normal organs and tissue show physiologically expression (*1-3*). Currently, ^{68}Ga-PSMA-11 is widely used as a primary imaging tool for PCA restaging using positron emission tomography (PET) at biochemical recurrence (*4,5*). It enables for a high detection rate of small soft-tissue and bone lesions even at low prostate specific antigen (PSA) values (*6*). The high and specific tumor uptake of ^{68}Ga-PSMA-11 prompted researchers to develop PSMA-ligands with a DOTA-chelator (e.g. PSMA-617), for labeling with ^{177}Lu for therapeutic applications (*7,8*). Off-target uptake of PSMA radioligands was commonly detected in kidneys, the duodenum and small bowel, as well as in the lacrimal and major salivary glands (*9*). First dosimetry studies of ^{177}Lu-PSMA-617 revealed a significantly higher mean absorbed dose in salivary glands (1.4 Gy/GBq) compared to kidney-doses (0.75 Gy/GBq) (*10*). This is in concordance with first results obtained after ^{177}Lu-PSMA-617 therapy, where no early nephrotoxicity, but some transient xerostomia in 8-20% patients was observed (*7,11*). High salivary gland uptake is of particular concern when PSMA-ligands are applied with α-particle emitters, such as ^{225}Ac, since this resulted in irreversible xerostomia and, hence, dose-limiting toxicity (*12,13*).

It was previously reported that PSMA is physiologically expressed on normal prostate epithelial cells, in the small intestine, renal tubular cells and the salivary glands, however, at much lower levels than in prostate cancer tissue (*13-15*). Other publications reported on immunohistochemical investigations which showed no PSMA expression in salivary glands (*2,16,17*). These findings were in agreement with the fact that PSMA-specific radioimmunoconjugates, such as ^{111}In-J591 and ^{177}Lu-J591, did not accumulate in salivary glands (*18*).

A previous comment on the importance of salivary gland toxicity in PSMA targeted radionuclide therapy stated the lack of sufficient data and understanding of the high uptake of PSMA-ligands (*19*).

Published mouse-experiments do not reveal high accumulation of PSMA-targeting radioligands in salivary gland tissue (*20,21*). Therefore, such models are not suitable to investigate radiotherapy related side effects to the salivary glands or methods to reduce salivary glands uptake of PSMA-targeting ligands.

The aim of this study was to compare the in vivo accumulation of ^{68}Ga-PSMA-11 in prostate cancer tissue, salivary glands and pancreas of patients to the PSMA expression levels on PCA patient tissue, as well as to benign salivary gland and pancreatic tissue using IHC and in vitro ARG.

MATERIALS AND METHODS

Patients for immunohistochemistry and autoradiography

Patients undergoing neck dissections including tumor-free submandibular glands (SMG) were prospectively selected. Tissue of patients that underwent pancreas resection were included for the analysis of benign pancreatic tissue. All patients with prostatectomy for PCA and preoperative ^{68}Ga-PSMA-11 PET/MRI available were screened, and cases with tumor in the apex were selected, as fresh frozen tissue after standard prostatectomy was only available from the apex. For PET quantification in normal tissue, patients referred to a ^{68}Ga-PSMA-11 PET for biochemical recurrence, were selected. All patients gave written informed consent to further analysis of their data and biological material within biobank protocols approved by the local ethics committee (BASEC No. 2016-00778, 2017-01319, KEK-StV-Nr: 40/08 and KEK-ZH-Nr. 06/08). The direct comparison to ^{68}Ga-PSMA-11 PET images was only possible for the PCA specimens. In order to determine the uptake of ^{68}Ga-PSMA-11 in prostate cancer relative to the uptake in salivary glands and pancreas an additional cohort of 60 patients that previously underwent a ^{68}Ga-PSMA-11 PET for biochemical recurrence was included in a retrospective analysis (Figure 1).

Tissue preparation, PSMA immunohistochemistry and evaluation

Fresh tissue of all types, obtained from the resection specimens immediately after surgery, was snap frozen. The remaining tissue was formalin-fixed, paraffin-embedded (FFPE) and examined on 2 µm-thick hematoxylin & eosin (H&E) stained sections. Both tissue types were compared microscopically to be representative. Immunohistochemical staining for PSMA was performed according to the protocol in the supplemental data. PSMA expression was evaluated using a three-tiered system (1+ weak, 2+ moderate, 3+ strong) and the area covered by staining was estimated. Immunoreactivity score (IRS) was calculated as following: IRS = IHC expression score multiplied by the area covered

(*22*). The area fraction and Gleason scores were determined according to the protocol in the supplemental data.

In vitro PSMA autoradiography

PSMA-617 (ABX GmbH, Germany) was labeled with no-carrier added ^{177}Lu (ITG GmbH, Germany) under standard labeling conditions as previously reported (supplemental data) (*20*). In vitro autoradiography was performed on frozen sections of patient tissue and mouse xenografts (highly PSMA-positive PC-3 PIP and PSMA-negative PC-3 flu tumors;supplemental data). In brief, buffer-treated sections were incubated with a solution of ^{177}Lu-PSMA-617 (1.5 MBq/mL in Tris-HCl buffer containing 1% BSA) with or without blocking agent (200 µM 2-(Phosphonomethyl)-pentandioic acid (2-PMPA, Sigma, USA) for 60 min at room temperature. After removal of the radioligand solution, the sections were washed according to the protocol (supplemental data). The air-dried sections were exposed to a phosphor imaging screen (Super Resolution, Perkin Elmer, USA) that were developed using a radiometric phosphor imager (Cyclone Plus Storage Phosphor System, Perkin Elmer, USA). The signal intensity on the autoradiographic images was quantified using the OptiQuant Acquisition software (Version 5.0, Perkin Elmer, USA). PC-3 PIP and PC-3 flu tumor xenograft sections were used as a positive or negative control, respectively. It is important to recognize that PSMA-transduced PC-3 (PC-3 PIP) tumors express PSMA reproducibly at levels much higher than pathophysiological PSMA-expression levels on human prostate cancer (*23*). The percentage signal intensity relative to the PC-3 PIP section (set to 100%) was calculated. The images were arranged for visual display using Adobe Photoshop (Version CS6, Adobe Systems, USA).

^{68}Ga-PSMA-11 PET/MRI

The nine patients with primary prostate cancer with corresponding tissue analysis underwent a ^{68}Ga-PSMA-11 PET for staging high risk prostate cancer between June 2016 and August 2017. For the second cohort of patients for PSMA PET image quantification 60

consequtive patients referred for ^{68}Ga-PSMA-11 PET for biochemical recurrence were selected. All patients underwent a clinical routine whole-body PET/MRI 60 min after injection of ^{68}Ga-PSMA-11 using a hybrid scanner (SIGNA PET/MR, GE Healthcare, Waukesha, WI, USA) as reported previously and described in detail in the supplements (*24*). To quantify ^{68}Ga-PSMA-11 uptake, a standardized volume of interest (VOI) was positioned in regular tissue of the parotid, submandibular, lacrimal, sublingual glands, as well as pancreatic, hepatic and splenic tissue to assess the maximum and mean standardized uptake value (SUV_{max} and SUV_{mean}). For patients with PSMA-positive local recurrence or metastasis a VOI was placed over the most active lesion.

To quantify PSMA uptake on ^{68}Ga-PSMA-11 PET images in the 9 primary tumors, VOIs were placed into the apical quadrant positive for cancer on histopathology that was selected for further ARG and IHC analysis.

Statistical analysis

Statistical analysis was performed with SPSS® 25.0.0.0 software (IBM®, Armonk, NY, USA). Descriptive statistics was used to display patient data as median, standard deviation (SD), or number (percent). The average activity or intensity on IHC, ARG and PET imaging was correlated with the values obtained for SMG, pancreas and PCA using Pearson correlation. A *P*-value lower than 0.05 was considered to indicate statistical significance. Linear regression was used between the signal intensity on ARG and the uptake on PSMA PET to estimate the relation between PSMA expression and tracer uptake on ^{68}Ga-PSMA-11 PET images.

RESULTS

Patient samples for analysis of PSMA expression on SMG were isolated from 9 consecutive patients, for pancreatic tissue from 4 patients and for PCA tissue from 9 patients with cancer in the apex. In 60 patients undergoing ^{68}Ga-PSMA-11 PET for restaging, the activity accumulation was determined in the lacrimal, parotid, submandibular and sublingual gland, as well as in pancreatic, splenic, hepatic tissue and in PCA lesions (Fig. 1, Table 1). In 31 patients, ^{68}Ga-PSMA-11-positive metastasis were clearly localized. The mean uptake in the submandibular glands was not different between patients with or without ^{68}Ga-PSMA-11-positive lesions with a SUV_{max} 23.5±5.2 vs. 23.3±5.1 (p=0.875), respectively.

Prostate cancer

Frozen tissue sections of the apex were analyzed in 9 patients with apical prostate cancer confirmed on H&E staining. The area fraction covered by adenocarcinoma on the slides ranged from 3% to 33% and included Gleason Scores from 3+3 to 4+4. The corresponding, paraffin-embedded tissue stained with an anti-PSMA antibody, indicated PSMA expression ranging from low (1+) to strong (3+), covering 70–100% of the tumor tissue with IRS values between 70 - 300 (Table 2).

In analogy to the IRS score, the signal intensity on ARG images of PCA tissue relative to PC-3 PIP tumor xenograft sections showed a heterogeneous pattern with a mean signal intensity of 8.5±6.8% and a range between 1.33 – 21.98% (Fig. 2A). The pattern of signal intensity on frozen sections corresponded well with the tumor region on H&E histology.

Also, the in vivo ^{68}Ga-PSMA-11 accumulation determined on PET scans showed a heterogeneous SUV_{max} ranging from 4.4 to 16.0 in the areas of the investigated primary prostate adenocarcinoma corresponding to the signal seen on ARG (Table 2, Fig. 3).

Pancreatic tissue

The healthy pancreatic tissue (PANC) was negative for PSMA on IHC in all four cases, even in the intercalated ducts (IRS 0; Table 3). The average signal intensity of the ARG performed on the pancreatic tissue was minimal in relation to PC-3 PIP tumor xenograft

sections (0.1±0.05%, supplemental Fig. S1), as was the case for the ^{68}Ga-PSMA-11 accumulation on ^{68}Ga-PSMA-11 PET scans that was low as well (SUV_{max} of 3.1±1.1) (Table 4).

Salivary glands

Three SMG were atrophic with signs of chronic inflammation, while six glands had a normal histology without inflammatory changes. IHC of PSMA expression showed distinct PSMA staining intensity (2 to 3+) that were very limited in extent (5% of the tissue) and typically confined to the intercalated ducts of normal SMG, yielding an IRS of 10 - 15. Atrophic SMG showed a similar pattern, but markedly reduced staining intensity (1+), as well as decreased coverage (IRS of 2 - 5 ; Table 3, Fig. 4a-b). A minor, opaque and inconsistent staining of the mucinous glands was regarded as an unspecific artefact.

The average relative signal intensity on ARG images of SMG was 1.34±0.89%. The three atrophic glands showed reduced signal intensity on ARG (0.14±0.1%) compared to the six glands with normal histology (1.94±0.32%) (Fig. 2B). Given the fact that most PCA patients do not have atrophic salivary glands, further comparison was performed by considering only the average uptake of healthy SMG (Table 3).

In contrast to the low IRS on IHC and the minimal signal intensity on ARG, all SMG on ^{68}Ga-PSMA-11 PET scans revealed a very strong accumulation of the tracer with a mean SUV_{max} of 23.5±5.2 (range 13.6 – 36.6) (Table 4, Fig. 5).

Correlation between IHC, ARG and PET

The IRS evaluated by IHC and the ARG intensity showed a significant correlation (R^2 = 0.642, p = 0.009), visualizing the areas of PSMA-positive prostate adenocarcinoma. Furthermore, the ARG intensity correlated well with the accumulation of ^{68}Ga-PSMA-11 in the apical quadrant of the prostate as determined on PET images (R^2 = 0.897, p < 0.001) (Fig. 6).

In addition, SMG and pancreatic tissue displayed a significant correlation between the low IRS (mean SMG 8.7±4.9 and mean PANC 0.0±0.0) and the low ARG signal intensity (mean SMG 1.3±0.9% and mean PANC 0.1±0.1%, R^2 = 0.739, p<0.001). In vivo accumulation of ^{68}Ga-PSMA-11 was very strong in SMG, with a mean SUV_{max} of 23.5±5.2 even surpassing the highest uptake detected in primary prostate adenocarcinoma (SUV_{max} 16.0 in PCA09) (Fig. 6).

Applying a linear fit algorithm for ARG signal intensity and SUV_{max}, over the 9 PCA cases, the following equation would result in (ARG %) = 1.46* (SUV_{max}) - 3.9. Assuming a similar perfusion between SMG tissue and prostate cancer tissue, the same function should be applicable for ARG signal intensity and SUV_{max} on SMG. As a consequence, a mean ^{68}Ga-PSMA-11 uptake of SUV_{max} 23.5 determined on PET scans would correspond to an average signal intensity of 30% ((1.46*23.5)-3.9) on ARG images. This would, however, be a 15-fold increased value as compared to the actual signal intensity of 1.9% determined for ARG images of normal SMG in our study.

DISCUSSION

The presented data support a mainly non-PSMA related radioligand uptake in salivary glands, in contrast to a significant correlation of PSMA mediated ligand uptake in primary PCA. IHC analysis showed a patchy and focal PSMA expression limited to the intercalated ducts in SMG, while serous acinar cells and striated ducts did not show PSMA expression. On the SMG specimens with chronic sialadenitis and atrophy, the IHC staining pattern was similar but overall less intense. These data were confirmed by ARG analysis which showed very low signal intensity on SMG tissue. The pancreatic tissue which has a similar histology as the SMG did not show any expression of PSMA on IHC and ARG, respectively. As the main structural difference between pancreatic tissue and SMG are the striated ducts (*25*). The substantial difference of PSMA radioligand uptake between these tissues may be attributed to the striated ducts. However, this would be most likely PSMA-unrelated, as no PSMA expression is observed in the striated ducts.

The consistently high uptake of PSMA radioligands in all seromucous glands of the head and neck was also confirmed by Klein Nulent et al. with a retrospective analysis of 30 patients (*26*). Together with previous observations of minimal to patchy PSMA expression on IHC (*2,16,27*), this supports the hypothesis that the accumulation of small molecule PSMA-targeting radioligands is at least partially non-specific (*19*).

This could also explain why the injection of botulinum toxin into the salivary gland, which leads to a transient reduction in salivary gland function, reduces the PSMA radioligand accumulation up to 64% (*28*). Some clinicians suggested local cooling to reduce radioligand accumulation, however, the reduction of SUV_{max} by this measure was only 15%, so that further investigation is needed before consideration of clinical routine use (*29*). The approach of using inhibitors of PSMA (e.g 2-PMPA), was found more successful in view of protecting the kidney from radiation damage (*30*), rather than the SMG, which was another finding supporting the hypothesis that the uptake of PSMA-ligands in salivary glands is mostly PSMA-unrelated.

The sink effect in patients with high tumor burden is a phenomenon that led to a reduced PSMA accumulation in salivary glands (*31*), however, in the patient selected for this study referred for staging or early biochemical reurrence, the tumor burden was not high enough to affect the radioactivity uptake in the salivary glands (*31*).

A potential limitation of the present study may be the fact that a direct comparison of the accumulation of PSMA radioligands in vivo, determined by PET examinations and in vitro using ARG of the same specimens for salivary gland and pancreatic tissue is not possible. Given the very consistent results for both pancreatic and normal submandibular gland tissue regarding ARG and IHC, as well as the consistently high PSMA radioligand accumulation in salivary glands of the head and neck and low radioligand uptake in the pancreas, we believe that the indirect comparison as presented in this study, is conclusive to confirm our hypothesis.

CONCLUSION

Our data strongly suggest that accumulation of PSMA-targeting radioligands in salivary gland tissue is mainly non-specific. Further studies will be necessary to investigate the exact mechanism of radioligand accumulation in order to develop new strategies to reduce radiotracer uptake in this dose-limiting tissues. This is in particular critical for radionuclide therapy using alpha-particle emitters with high linear energy transfer.

Financial disclosure:

IAB has received research grants from GE Healthcare and Swiss Life and speaker honorarium from GE Healthcare, Bayer Health Care and Astellas Pharma AG. Authors NJR, CAU, DP, DL, AT, JM, UJM, DAF, MM, GM, GFH, DE and CM declare no conflict of interest.

The Department of Nuclear Medicine holds an institutional research contract with GE Healthcare. The authors thank the Sick legat and the Iten-Kohaut foundation for their financial support.

Acknowledgements

The authors acknowledge the technicians Marlena Hofbauer, Miguel Porto, Sofia Kaltsuni and Sabrina Epp for their work on high quality PET/MR scans. We thank Susanne Dettwiler, Fabiola Prutek and Christiane Mittmann for tissue processing and immunohistochemical stainings.

Tables:

Table 1 Patient characteristics

	N/mean	(%)/SD
Submandibular gland:	**9**	
Age (years)	59	±13
Previous RTX (yes)	3	33%
Pancreatic tissue:	**4**	
Age (years)	66	±18
PCa-tissue:	**9**	
Age (years)	63	±5.4
Prostate cancer (+)	9	100%
PSMA-PET scans:	**60**	
Age (years)	67.3	±6.9
Dose (MBq)	136	±14.0
Weight (kg)	84.3	±10.8
Number of PCa metastasis	31	

Table 2 Comparison of the 9 primary prostate tumors (PCa) on histology, autoradiography (ARG) and PSMA-PET: Gleason Score (GS), carcinoma covered area of the slide (covered area), predominant IHC intensity, percentage of carcinoma showing the predominant intensity, Immunoreactivity score (IRS; predominant intensity x percentage of staining); relative signal intensity on ARG, in vivo accumulation of ^{68}Ga-PSMA-11 (SUV_{max}/SUV_{mean}).

Case:	GS	H&E PCa-covered area (%)	PSMA IHC Intensity	PSMA IHC % of Tumor	PSMA IHC IRS	ARG (%)	PSMA SUV_{max}	PSMA SUV_{mean}
PCA 01	3+4	13	1	70	70	1.3	4.4	2.9
PCA 02	4+4	13	2	80	160	2.5	5.3	3.2
PCA 03	3+3	17	1	80	80	2.6	3.3	2.9
PCA 04	3+4	28	3	70	210	4.5	4.7	3.1
PCA 05	3+4	33	2	80	160	6.7	9.2	8.1
PCA 06	3+4	32	3	100	300	8.8	7.5	5.7
PCA 07	3+4	3	3	100	300	10.6	12.6	7.5
PCA 08	4+4	20	3	100	300	17.6	13.9	11.6
PCA 09	4+4	19	3	100	300	22.0	16	8.8

Table 3: Comparison of the 9 salivary gland and 4 pancreatic tissues: histology, PSMA expression intensity, percentage of tissue stained and immunoreactivity score (IRS; intensity x % staining) and relative signal intensity on ARG.

Case:	Histology	PSMA IHC Intensity	PSMA IHC % of tissue	PSMA IHC IRS	ARG (%)
SMG 01	atrophic	1	5	5	0.1
SMG 02	atrophic	1	2	2	0.2
SMG 03	atrophic	1	2	2	0.1
SMG 04	normal	2	5	10	1.9
SMG 05	normal	3	5	15	1.4
SMG 06	normal	3	5	15	1.9
SMG 07	normal	2	5	10	2.2
SMG 08	normal	2	5	10	1.8
SMG 09	normal	2	5	10	2.4
PANC 01	normal	0	0	0	0.0
PANC 02	normal	0	0	0	0.1
PANC 03	normal	0	0	0	0.2
PANC 04	normal	0	0	0	0.1

Table 4. Quantification of ^{68}Ga-PSMA-11 accumulated in different tissues based on PSMA-PET. (SD = Standard deviation)

Tissue activity on PSMA PET (SUV_{max})					
	N	Minimum	Maximum	Mean	SD
Parotid	60	10.0	30.4	**19.8**	4.7
Submandibular	60	13.6	36.6	**23.5**	5.2
Lacrimal	60	6.0	25.8	**13.8**	4.2
Sublingual	60	3.6	31.0	**10.7**	4.6
Tonsils	60	3.0	12.6	**7.8**	2.1
Pancreas	60	0.4	5.4	**3.1**	1.1
Liver	60	4.1	16.3	**8.2**	2.6
Spleen	60	5.0	21.0	**11.2**	3.9
PCA-tissue	31	2.7	48.7	**15.9**	11.8

Figures:

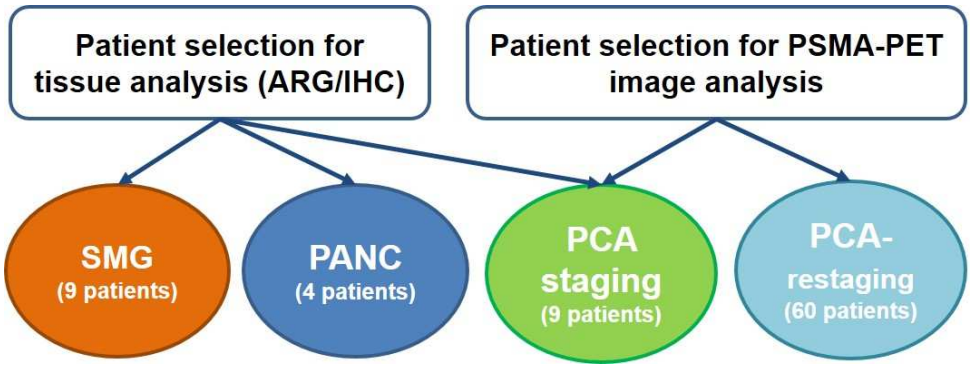

Figure 1: Overview of selected patients for tissue collection for autoradiography (ARG) and immunohistochemistry (IHC) (submandibular glands (SMG 01-09), pancreas (PANC 01-04) and primary prostate cancer (PCA 01-09)), as well as PSMA PET quantification, including the 9 patients with primary prostate cancer (PCA01-09) and 60 patients referred for restaging for the analysis of average uptake on salivary glands, pancreas, spleen, liver and prostate cancer metastasis.

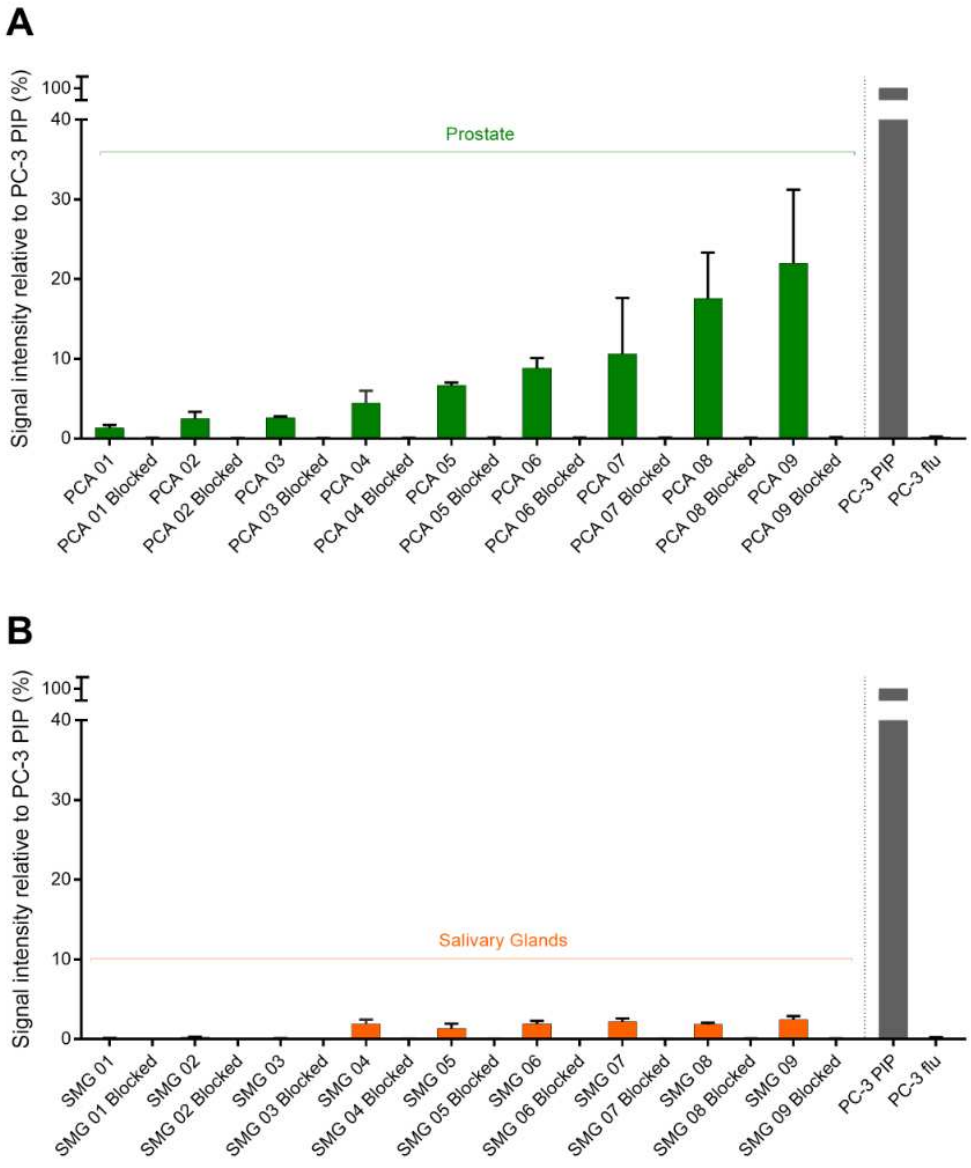

Figure 2: (A) Autoradiography quantification of signal intensity of human primary prostate cancer (PCA) tissue relative to PC-3 PIP (high PSMA expression, set to 100%) and PC-3 flu (low PSMA expression) mouse tumor xenograft sections after the application of ^{177}Lu-PSMA-617. Data shown for unblocked and 2-PMPA-blocked tissue sections. A heterogeneous pattern of signal intensity on ARG was observed with a mean of 8.5±6.8%, range 1.33 – 21.98% compared to PC-3 PIP tumor tissue. (B) Same ARG qunatification for human salivary gland sections. SMG 01-03 with atrophy showed only minimal signal

intensity (0.14±0.10%) and SMG 04-09 with normal histology showed low signal intensity (1.94±0.32%).

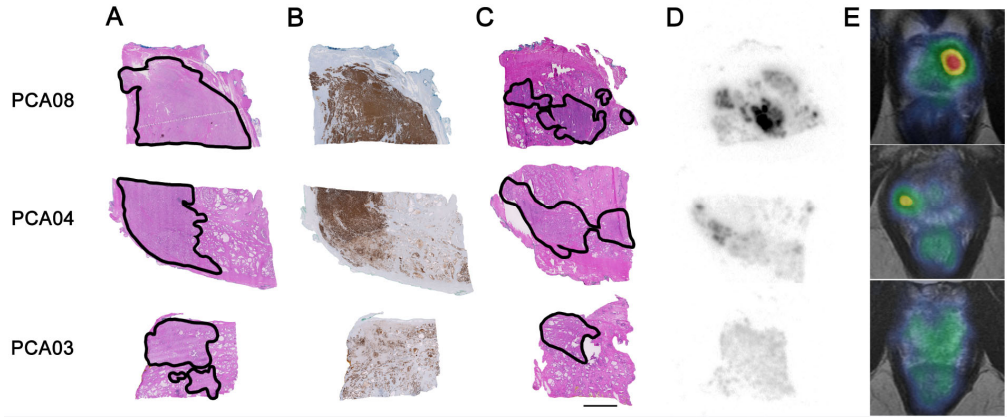

Figure 3: Comparison of three selected examples of prostate carcinomas (line by line) regarding H&E histology, PSMA IHC, in vitro ARG and in vivo PET. (A) shows encircled carcinoma areas in formaline fixed tissue, (B) the respective corresponding PSMA immunohistochemisty and (C) the selected encircled carcinoma areas in the fresh frozen tissue (scale bar 5 mm). (D) depicts the corresponding in vitro autoradiography with high (PCA08, GS 4+4), moderate (PCA04, GS 3+4) and low (PCA03, GS 3+3) normalized signal intensity on ARG, whereas (E) shows corresponding axial slice through the apex of the prostate on PSMA PET/MR.

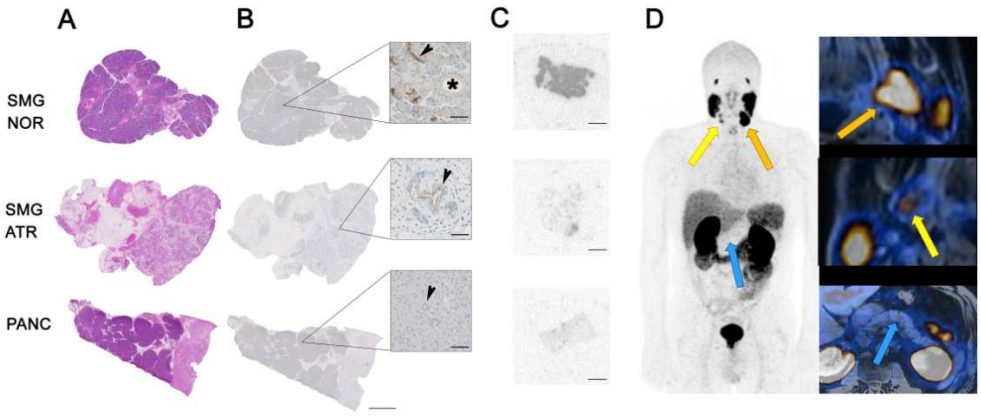

Figure 4: Comparison of normal and atrophic submandibular salivary gland tissue (SMG NOR and ATR), and pancreatic tissue (PANC) regarding H&E histology, PSMA IHC and in vivo PET. (A) H&E histology of these three tissue types. (B) Moderate, but focal PSMA expression in intercalated ducts (inset, arrow), whereas striated ducts (inset, asterisk) are PSMA negative and intercalated ducts of atrophic salivary gland tissue show less expression. In pancreatic tissue, no PSMA expression is noted (inset, arrow shows negative intercalated duct). Scale bar 5 mm, and 100 µm (insets). (C) depicts in vitro ARG with normalized signal intensity for normal and atrophic SMG besides normal pancreatic tissue. Scale bar 5 mm. (D) PSMA PET scan of a patient showing high PSMA accumulation in the left submandibular gland (orange arrow, SUV_{max} 33), lower uptake in the atrophic right submandibular gland (yellow arrow, SUV_{max} 11) and only minimal uptake in the pancreas (blue arrow, SUV_{max} 3) (magnification in insets).

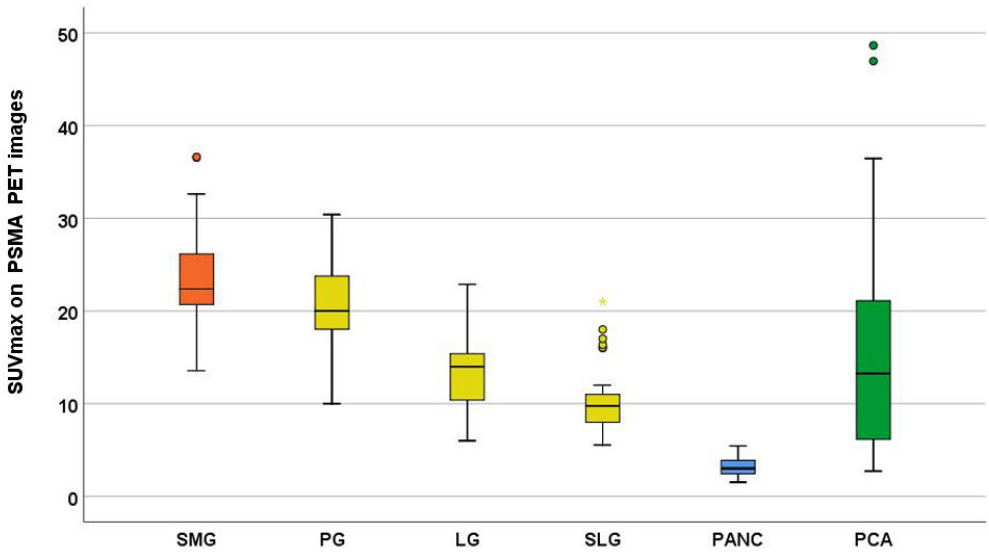

Figure 5: Box plots illustrating the PSMA-PET activity distribution for 60 consecutive patients imaged for PCA recurrence. High accumulation of ^{68}Ga-PSMA-11 60 minutes after injection can be measured in the salivary glands of the head and neck area, with a maximum in submandibular glands (SMG, orange), followed by parotid gland (PG), lacrimal gland (LG) and sublingual gland (SLG). Only minimal uptake was determined in the pancreatic tissue (PANC, blue). The average ^{68}Ga-PSMA-11 uptake in the submandibular glands was higher compared to the uptake in prostate cancer metastasis (PCA, green).

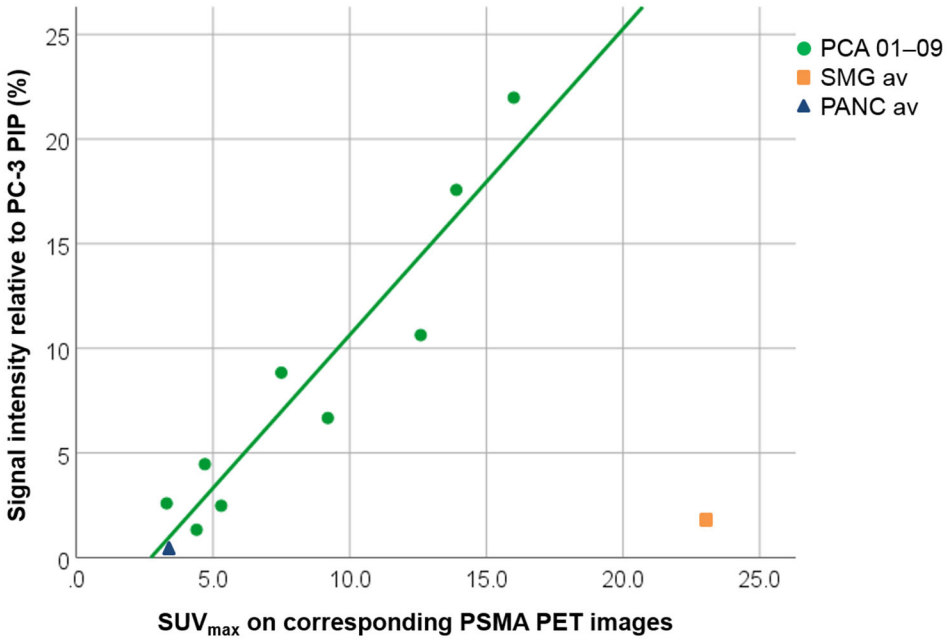

Figure 6: Scatter plot with linear regression fit for the quantification of the relative signal intensity on ARG images and the corresponding quantification of the in vivo uptake of ^{68}Ga-PSMA-11 on PET images (SUV_{max}) for prostate cancer (PCA) specimens (green, circle), with a linear regression fit (R^2 = 0.897, $p < 0.001$, $y = 1.46*x - 3.9$). The average ARG signal intensity for salivary glands (SMG_{nor} ,1.94%) in relation to the average SUV_{max} on 60 PSMA PET scans (SUV_{max} 23.5) is shown in orange (square) and the ARG signal intensity for the pancreases (PANC; 0.1%) in relation to the average SUV_{max} on 60 PSMA PET scans (SUV_{max} 3.1) in blue (triangle).

References:

1. Wright GL, Jr., Haley C, Beckett ML, Schellhammer PF. Expression of prostate-specific membrane antigen in normal, benign, and malignant prostate tissues. *Urol Oncol.* 1995;1:18-28.

2. Silver DA, Pellicer I, Fair WR, Heston WD, Cordon-Cardo C. Prostate-specific membrane antigen expression in normal and malignant human tissues. *Clin Cancer Res.* 1997;3:81-85.

3. Perner S, Hofer MD, Kim R, et al. Prostate-specific membrane antigen expression as a predictor of prostate cancer progression. *Hum Pathol.* 2007;38:696-701.

4. Afshar-Oromieh A, Avtzi E, Giesel FL, et al. The diagnostic value of PET/CT imaging with the ^{68}Ga-labelled PSMA ligand HBED-CC in the diagnosis of recurrent prostate cancer. *Eur J Nucl Med Mol Imaging.* 2015;42:197-209.

5. Afshar-Oromieh A, Holland-Letz T, Giesel FL, et al. Diagnostic performance of 68Ga-PSMA-11 (HBED-CC) PET/CT in patients with recurrent prostate cancer: evaluation in 1007 patients. *Eur J Nucl Med Mol Imaging.* 2017;44:1258-1268.

6. Kranzbuhler B, Nagel H, Becker AS, et al. Clinical performance of (68)Ga-PSMA-11 PET/MRI for the detection of recurrent prostate cancer following radical prostatectomy. *Eur J Nucl Med Mol Imaging.* 2018;45:20-30.

7. Rahbar K, Ahmadzadehfar H, Kratochwil C, et al. German Multicenter Study Investigating 177Lu-PSMA-617 Radioligand Therapy in Advanced Prostate Cancer Patients. *J Nucl Med.* 2017;58:85-90.

8. Okamoto S, Thieme A, Allmann J, et al. Radiation dosimetry for ^{177}Lu-PSMA I&T in metastatic castration-resistant prostate cancer: absorbed dose in normal organs and tumor lesions. *J Nucl Med.* 2017;58:445-450.

9. Herrmann K, Bluemel C, Weineisen M, et al. Biodistribution and radiation dosimetry for a probe targeting prostate-specific membrane antigen for imaging and therapy. *J Nucl Med.* 2015;56:855-861.

10. Kratochwil C, Giesel FL, Stefanova M, et al. PSMA-Targeted Radionuclide Therapy of Metastatic Castration-Resistant Prostate Cancer with 177Lu-Labeled PSMA-617. *J Nucl Med.* 2016;57:1170-1176.

11. Ahmadzadehfar H, Rahbar K, Kurpig S, et al. Early side effects and first results of radioligand therapy with ^{177}Lu-DKFZ-617 PSMA of castrate-resistant metastatic prostate cancer: a two-centre study. *EJNMMI Res.* 2015;5:114.

12. Kratochwil C, Bruchertseifer F, Giesel FL, et al. 225Ac-PSMA-617 for PSMA-Targeted alpha-Radiation Therapy of Metastatic Castration-Resistant Prostate Cancer. *J Nucl Med.* 2016;57:1941-1944.

13. Kratochwil C, Bruchertseifer F, Rathke H, et al. Targeted alpha-Therapy of Metastatic Castration-Resistant Prostate Cancer with (225)Ac-PSMA-617: Dosimetry Estimate and Empiric Dose Finding. *J Nucl Med.* 2017;58:1624-1631.

14. Israeli RS, Powell CT, Corr JG, Fair WR, Heston WD. Expression of the prostate-specific membrane antigen. *Cancer Res.* 1994;54:1807-1811.

15. Troyer JK, Beckett ML, Wright GL, Jr. Detection and characterization of the prostate-specific membrane antigen (PSMA) in tissue extracts and body fluids. *Int J Cancer.* 1995;62:552-558.

16. Mhawech-Fauceglia P, Zhang S, Terracciano L, et al. Prostate-specific membrane antigen (PSMA) protein expression in normal and neoplastic tissues and its sensitivity and specificity in prostate adenocarcinoma: an immunohistochemical study using mutiple tumour tissue microarray technique. *Histopathology.* 2007;50:472-483.

17. Chang SS, Reuter VE, Heston WD, Bander NH, Grauer LS, Gaudin PB. Five different anti-prostate-specific membrane antigen (PSMA) antibodies confirm PSMA expression in tumor-associated neovasculature. *Cancer Res.* 1999;59:3192-3198.

18. Pandit-Taskar N, O'Donoghue JA, Morris MJ, et al. Antibody mass escalation study in patients with castration-resistant prostate cancer using 111In-J591: lesion detectability and dosimetric projections for 90Y radioimmunotherapy. *J Nucl Med.* 2008;49:1066-1074.

19. Taieb D, Foletti JM, Bardies M, Rocchi P, Hicks RJ, Haberkorn U. PSMA-Targeted Radionuclide Therapy and Salivary Gland Toxicity: Why Does It Matter? *J Nucl Med.* 2018;59:747-748.

20. Umbricht CA, Benesova M, Schmid RM, et al. (44)Sc-PSMA-617 for radiotheragnostics in tandem with (177)Lu-PSMA-617-preclinical investigations in comparison with (68)Ga-PSMA-11 and (68)Ga-PSMA-617. *EJNMMI Res.* 2017;7:9.

21. Banerjee SR, Pullambhatla M, Foss CA, et al. (6)(4)Cu-labeled inhibitors of prostate-specific membrane antigen for PET imaging of prostate cancer. *J Med Chem.* 2014;57:2657-2669.

22. Remmele W, Stegner HE. [Recommendation for uniform definition of an immunoreactive score (IRS) for immunohistochemical estrogen receptor detection (ER-ICA) in breast cancer tissue]. *Pathologe.* 1987;8:138-140.

23. Umbricht CA, Benesova M, Schibli R, Muller C. Preclinical Development of Novel PSMA-Targeting Radioligands: Modulation of Albumin-Binding Properties To Improve Prostate Cancer Therapy. *Mol Pharm.* 2018;15:2297-2306.

24. Sekine T, Barbosa FG, Sah BR, et al. PET/MR Outperforms PET/CT in Suspected Occult Tumors. *Clin Nucl Med.* 2017;42:e88-e95.

25. Orstavik TB, Brandtzaeg P, Nustad K, Pierce JV. Immunohistochemical localization of kallikrein in human pancreas and salivary glands. *J Histochem Cytochem.* 1980;28:557-562.

26. Klein Nulent TJW, Valstar MH, de Keizer B, et al. Physiologic distribution of PSMA-ligand in salivary glands and seromucous glands of the head and neck on PET/CT. *Oral Surg Oral Med Oral Pathol Oral Radiol.* 2018;125:478-486.

27. Gong MC, Chang SS, Sadelain M, Bander NH, Heston WD. Prostate-specific membrane antigen (PSMA)-specific monoclonal antibodies in the treatment of prostate and other cancers. *Cancer Metastasis Rev.* 1999;18:483-490.

28. Baum RP, Langbein T, Singh A, et al. Injection of Botulinum Toxin for Preventing Salivary Gland Toxicity after PSMA Radioligand Therapy: an Empirical Proof of a Promising Concept. *Nucl Med Mol Imaging.* 2018;52:80-81.

29. van Kalmthout LWM, Lam M, de Keizer B, et al. Impact of external cooling with icepacks on (68)Ga-PSMA uptake in salivary glands. *EJNMMI Res.* 2018;8:56.

30. Kratochwil C, Giesel FL, Leotta K, et al. PMPA for nephroprotection in PSMA-targeted radionuclide therapy of prostate cancer. *J Nucl Med.* 2015;56:293-298.

31. Gaertner FC, Halabi K, Ahmadzadehfar H, et al. Uptake of PSMA-ligands in normal tissues is dependent on tumor load in patients with prostate cancer. *Oncotarget.* 2017;8:55094-55103.

SUPPLEMENTAL DATA

METHODS

Tissue preparation, PSMA immunohistochemistry and evaluation

Fresh tissue of all types, obtained from the resection specimens immediately after surgery, was snap frozen. The remaining tissue was formalin-fixed, paraffin-embedded (FFPE) and examined on 2 µm-thick hematoxylin & eosin (H&E) stained sections. Immunohistochemical staining was performed on additional 2 µm-thick sections using the Ventana Benchmark (Roche Ventana Medical Systems, Inc., Tucson, AZ, USA) automated staining system. A primary antibody directed against the extracellular domain of PSMA (DAKO, M3620, clone 3E6, 1:25) was used. Detection was performed with optiView DAB-kit (Ventana). Slides were counterstained with hematoxylin (Ventana). PSMA expression was evaluated using a three-tiered system (1+ weak, 2+ moderate, 3+ strong) and the area covered by staining was estimated in the following scale (1%, 2%, 5%, 10% followed by further 10% steps). Immunoreactivity score (IRS) was calculated as following: IRS = IHC expression score multiplied by the area covered (*1*). The area fraction covered by carcinoma on the H&E slides was determined after digitalization of the slides (Nanozoomer NDP digital slide scanner C9600-12 by Hamamatsu) using the Hamamatsu NDP.view 2.6.8 Software. The Gleason scores and carcinoma areas were evaluated on each corresponding slide by an experienced genitourinary pathologist (N.J.R.).

^{177}Lu-labeling of PSMA-617

No-carrier added ^{177}Lu was obtained from Isotope Technologies Garching (ITG GmbH, Garching, Germany). Radiolabeling of PSMA-617 was performed at a specific activity of 100 MBq/nmol. Therefore, the compound was incubated at 95°C with $^{177}LuCl_3$ and a solution of HCl (0.05 M) and Na-acetate (0.5 M) at pH ~ 4 for 10 minutes. Quality control was performed by high performance liquid chromatography (HPLC, Merck Hitachi,

Darmstadt, Germany) with a C-18 reversed phase column (XTerraTM MS C-18, 5 µm, 15 cm x 4.6 cm, Waters, Milford, MA, U.S.) and a radio flow detector LB508 (Berthold Technologies). The mobile phase consisted of MilliQ water with 0.1% trifluoroacetic acid (A) and acetonitrile (B) with a linear gradient from 5% to 80% B over 15 min at a flow rate of 1 mL/min. The radioligand was used for AR studies at radiochemical yields >98% without further purifications.

In vitro PSMA autoradiography

PSMA-617 (ABX GmbH, Germany) was labeled with no-carrier added ^{177}Lu (ITG GmbH, Germany) under standard labeling conditions as previously reported (*2*). In vitro autoradiography was performed on frozen sections of patient tissue and mouse xenografts (PC-3 PIP and PC-3 flu tumor xenografts grown in BALB/c nude mice to serve as positive and negative controls, respectively) and immobilized on Superfrost Plus slides (Adhesion slides, Thermo Scientific, Germany). The slides with tissue sections were pre-incubated in Tris-HCl buffer (170 mM, pH 7.6, with 5 mM $MgCl_2$) containing 0.25% (w/v) bovine serum albumin (BSA, Sigma, USA) for 10 min at room temperature. The sections were then incubated with a solution of ^{177}Lu-PSMA-617 (1.5 MBq/mL in Tris-HCl buffer containing 1% BSA) with or without blocking consisting of 200 µM 2-(Phosphonomethyl)-pentandioic acid (2-PMPA, Sigma, USA) for 60 min at room temperature. After removal of the radioligand solution, the sections were washed twice for 5 min in cold Tris-HCl buffer (with 0.25% BSA), then twice for 5 min in pure Tris-HCl buffer, and finally rinsed with cold distilled water. The sections were air-dried followed by exposure to a phosphor imaging screen (Super Resolution, Perkin Elmer, USA). The screens were developed using a radiometric phosphor imager (Cyclone Plus Storage Phosphor System, Perkin Elmer, USA). The signal intensity on the autoradiographic images was quantified by contouring each sample using the OptiQuant Acquisition software (Version 5.0, Perkin Elmer, USA). PC-3 PIP and PC-3 flu tumor xenograft sections (cells kindly provided by Prof. Dr. Martin Pomper, John Hopkins Institutions, Baltimore, USA) were co-exposed and used as a positive or negative control,

respectively. The percentage signal intensity relative to the PC-3 PIP section (PC-3 PIP set to 100%) was calculated using digital light units per area (mm^2). The files generated by the OptiQuant Acquisition software were opened and arranged for visual display using Adobe Photoshop (Version CS6, Adobe Systems, USA).

^{68}Ga-PSMA-11 PET/MRI

All patients underwent a clinical routine whole-body PET/MRI 60 min after injection of ^{68}Ga-PSMA-11 using a hybrid scanner (SIGNA PET/MR, GE Healthcare, Waukesha, WI, USA). For attenuation correction a 3D dual-echo, spoiled gradient recalled echo sequence (LAVA-FLEX) was acquired, and PET emission scans were recorded in list mode for 2 minutes per bed. The MR-based attenuation correction algorithm uses an atlas for the patient's head region. In the other anatomical regions, air, lung and soft tissue were segmented and a continuous fat/water-based attenuation correction method was applied(*3*). Furthermore, a high resolution T1-weighted LAVA-FLEX sequence, diffusion weighted images (b values: 0, 300, 1000) and a T2-weighted fast recovery fast spin echo (FRFSE) sequences in two planes were included for the pelvis. To reduce ^{68}Ga-PSMA-11 activity in the bladder, ureters and kidneys, furosemide (0.13 mg/kg) was injected intravenously 30 minutes prior to the ^{68}Ga-PSMA-11 injection, and patients were asked to void the bladder prior to the scan (*4*).

RESULTS

In vitro PSMA autoradiography

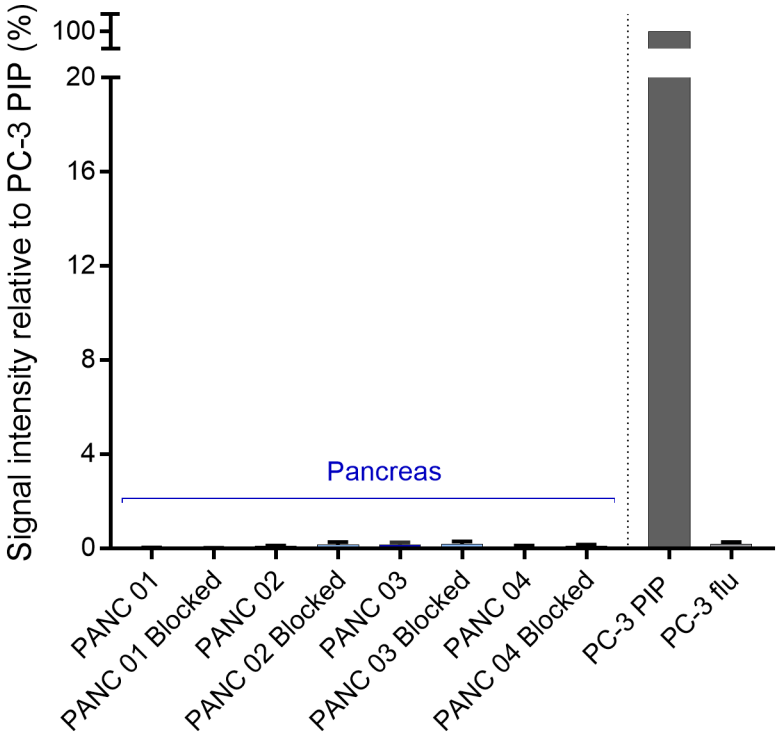

Fig. S1 Quantification of the signal intensity of human pancreatic tissue relative to PC-3 PIP (high PSMA expression, set to 100%) and PC-3 flu (low PSMA expression) tumor xenograft sections after the application of ^{177}Lu-PSMA-617. Data shown for unblocked and 2-PMPA-blocked tissue sections. All PANC tissue sections showed only minimal signal intensity (0.1±0.05%)

REFERENCE

1. Remmele W, Stegner HE. [Recommendation for uniform definition of an immunoreactive score (IRS) for immunohistochemical estrogen receptor detection (ER-ICA) in breast cancer tissue]. *Pathologe.* 1987;8:138-140.

2. Umbricht CA, Benesova M, Schmid RM, et al. (44)Sc-PSMA-617 for radiotheragnostics in tandem with (177)Lu-PSMA-617-preclinical investigations in comparison with (68)Ga-PSMA-11 and (68)Ga-PSMA-617. *EJNMMI Res.* 2017;7:9.

3. Wollenweber SD, Ambwani S, Lonn AHR, et al. Comparison of 4-Class and Continuous Fat/Water Methods for Whole-Body, MR-Based PET Attenuation Correction. *Ieee Transactions on Nuclear Science.* 2013;60:3391-3398.

4. Pizzuto DA, Muller J, Muhlematter U, et al. The central zone has increased (68)Ga-PSMA-11 uptake: "Mickey Mouse ears" can be hot on (68)Ga-PSMA-11 PET. *Eur J Nucl Med Mol Imaging.* 2018;45:1335-1343.

The Journal of NUCLEAR MEDICINE

First clinico-pathological evidence of a non PSMA-related uptake mechanism for ^{68}Ga-PSMA-11 in salivary glands.

Niels J. Rupp, Christoph A. Umbricht, Daniele A. Pizzuto, Daniela Lenggenhager, Antonia Töpfer, Julian Müller, Urs Jacob Mühlematter, Daniela A. Ferraro, Michael Messerli, Grégoire B. Morand, Gerhard F. Huber, Daniel Eberli, Roger Schibli, Roger Schibli and Irene A. Burger

J Nucl Med.
Published online: February 8, 2019.
Doi: 10.2967/jnumed.118.222307

The Journal of Nuclear Medicine is published monthly.
SNMMI | Society of Nuclear Medicine and Molecular Imaging
1850 Samuel Morse Drive, Reston, VA 20190.
(Print ISSN: 0161-5505, Online ISSN: 2159-662X)

SNMMI SOCIETY OF NUCLEAR MEDICINE AND MOLECULAR IMAGING